Investigation of one-neutron transfer in $^{13}C + ^{27}Al$ at $E_{lab} = 32$ MeV

B. R. Gonçalves,[1,*] D. R. Mendes Junior,[1] R. Linares,[1] V. A. B. Zagatto,[1] C. C. Seabra,[1] L. R. Gasques,[2] V. Scarduelli,[2] J. C. Zamora,[3,2] L. C. Chamon,[2] and A. Lépine-Szily[2]

[1]*Instituto de Física, Universidade Federal Fluminense, 24210-340 Niterói, Rio de Janeiro, Brazil*

[2]*Instituto de Física, Universidade de São Paulo, C. P. 66318, 05389-970 São Paulo, Brazil*

[3]*Facility for Rare Isotope Beams, Michigan State University, East Lansing, Michigan 48824, USA*

(Received 1 January 2024; accepted 23 February 2024; published 4 April 2024)

The $^{13}C + ^{27}Al$ reaction ($E_{lab} = 32$ MeV) has been measured, and the elastic scattering, target excitation, and one-neutron transfer channels have been investigated. A comparison of the data with the results of different theoretical frameworks indicates the necessity of including the effect of the spin-orbit interaction of the target to properly reproduce the data. The inclusion of the one-neutron transfer did not significantly affected the elastic angular distribution. The one-neutron transfer reaction could be well reproduced when the *psdmod* interaction was used to describe the $^{27,28}Al$ nuclei and their associated features. The results reported here are consistent with those previously reported for the $^{13}C + ^{28}Si$ reaction measured at similar bombarding energies, providing further evidence of the similarities between these nuclei.

DOI: 10.1103/PhysRevC.109.044608

I. INTRODUCTION

In nuclear collisions, the structure of the colliding partners affects the yields observed in the subsequent reaction channels. Therefore, accurate knowledge of the reaction dynamics allows access to the nuclear structure information of the colliding nuclei. Some reactions are more suitable to reach specific pieces of information about the nuclear structure such as one-nucleon transfer, in which the single-particle nature of the nuclear wave function is in the foreground.

The (d, p) [1,2] and (t, d) [3] are two examples of one-neutron transfer reactions often adopted to study the nuclear structure between nuclei with masses A and $A + 1$. Within the direct reaction models, the one-neutron transfer cross sections are related to the overlap function, built from the wave function for a given state in the involved nuclei. Deviations between experimental and theoretical [typically obtained via distorted wave Born approximations (DWBA) calculations] cross sections are usually accounted on the so-called spectroscopic factor $\mathcal{S}$. This factor can be compared with values obtained from nuclear structure models like the shell model. However, ambiguities in the experimentally based $\mathcal{S}$ may be observed due to incomplete modeling of the reaction mechanism. In the case of (d, p) reaction, breakup can be a relevant channel [4] and the reaction model may consider it.

It is assumed that the properties of nuclear structure remain the same regardless of the reaction used to probe it. In the context of one-neutron transfers, this assumption indicates that the same $\mathcal{S}$ between the A and $A + 1$ nuclei can also be assessed via (^{7}Li, ^{6}Li), (^{13}C, ^{12}C), and other heavy-ion reactions. Although intercomparisons between $\mathcal{S}$ from light- and heavy-ion induced reactions seem to be an approach to refine the accuracy of $\mathcal{S}$, one should always consider that in heavy-ion induced reactions many channels and partial waves often contribute to the relevant cross sections. This calls for measurements of as many as possible reaction cross sections (a multichannel approach), like the elastic, inelastic, transfer, and breakup (when needed), and a consistent theoretical model to describe the experimental data. In the calculations, constraints on the optical potential and deformation parameters are imposed to simultaneously reproduce the elastic and inelastic cross sections. Couplings to the transfer channels are included using these consistent optical potentials and spectroscopic amplitudes from shell model calculations. The multichannel approach has been widely adopted within the NUMEN [5] project, aimed at obtaining relevant spectroscopic information for the neutrinoless double beta decay from heavy-ion induced double charge exchange reactions.

In recent works, this approach has also been applied to study the elastic, inelastic and transfer reactions induced by ^{6,7}Li on ^{120}Sn [6–8] and ^{124}Sn [9]. Since ^{6,7}Li are weakly bound nuclei, couplings to the breakup channel are important for the correct description of the several reaction channels observed. A complete reaction model including elastic, inelastic, transfer, and continuum coupling channels (breakup) is beyond the possibilities that the current computational codes for direct reactions can provide. One solution may be to include the couplings the continuum adopting a dynamic polarization potential derived from the continuum discretized coupled-channel formalism. In addition, the choice of optical potentials is of great importance and a systematic analysis of reactions involving ^{6,7}Li can be found in Ref. [10].

The (^{13}C, ^{12}C) reaction is an interesting one-neutron transfer probe because the projectile can be regarded as a single-valence neutron in a $1p_{1/2}$ bound to the ^{12}C nucleus

*brunarg@id.uff.br

with $S_n = 4.95$ MeV and, therefore, couplings to breakup channels are expected to be weak enough to be neglected. In a previous work, we applied the multichannel approach to the $^{13}C + ^{28}Si$ system [11]. Two shell model interactions for the relevant spectroscopic amplitudes for the $^{28,29}Si$ isotopes were considered: the so-called *psdmod* [12] and the *psdmwkpn* [13] interactions. As result, the measured cross sections for the one-neutron transfer in the $^{13}C + ^{28}Si$ system have a better agreement with the calculated angular distributions by using the spectroscopic amplitudes as obtained from the *psdmod* interaction.

The present manuscript extends the previous work on the $^{13}C + ^{28}Si$ to the $^{13}C + ^{27}Al$ system. The ground state of the ^{27}Al nucleus is often interpreted as a $1d_{5/2}$ proton hole in the ^{28}Si [14]. This suggest that the *psdmod* interaction can provide good results for the description of the one-neutron transfer cross sections.

This paper is organized as follows. Section II provides details of the experimental procedures employed in this measurement. Section III covers the theoretical framework, the calculations, and a discussion of their results in comparison with the experimental data set. Finally, the last section presents the main conclusions.

II. EXPERIMENTAL DETAILS

The experiment was performed at the *Laboratório Aberto de Física Nuclear* (LAFN) of the University of São Paulo (USP). The ^{13}C beam was produced from a 95% enriched ^{13}C cathode loaded into the NEC SNICS (source of negative ions by cesium sputtering) ion source. ^{13}C ions were accelerated up to an energy of 32 MeV by the 8-MV Tandem accelerator of the LANF facility. The ME-200 dipole magnet selected the ions and delivered the beam to the scattering chamber. Measurements at $E_{lab} = 32.0$ MeV were carried out with a typical $^{13}C^{+4}$ beam current of ≈50 nAe. A target ladder in the scattering chamber was mounted with two self-supported foils: i) a thin ^{27}Al foil and ii) a stacked ^{27}Al and ^{197}Au foil, for normalization purposes. Both targets were produced by deposition under vacuum with thicknesses between 20 μg/cm^2 and 30 μg/cm^2.

The *Silicon Array and Telescopes of USP for Reactions and Nuclear Applications* (SATURN) system [15] assembled with three ΔE-E telescopes were mounted on a rotating platform at 10° apart from each other. The ΔE detectors have a nominal thickness of 15–20 μm whereas the E detectors are 1000 μm thick. The rotating platform was set at four angles, covering an angular range between $25° \leqslant \theta_{lab} \leqslant 62°$. Figure 1 presents a typical ΔE-E spectrum at $\theta_{lab} = 25°$ obtained for measurements with the ^{27}Al target. The atomic species between α and nitrogen are clearly observed although particle identification does not allow to distinguish between $^{12,13}C$ isotopes and therefore the two-body kinematics is explored for identification of the reaction channels.

Carbon particles are selected in the ΔE-E spectrum and projected into a Q-value spectrum, defined as $Q = E_{total}(\theta) - E_{elas}(\theta)$, where $E_{elas}(\theta)$ is the energy of the elastic peak at the measured angle θ_{lab}. Figure 2 displays the Q-value spectrum for $\theta_{lab} = 35°$. In this representation, the peak at $Q = 0$

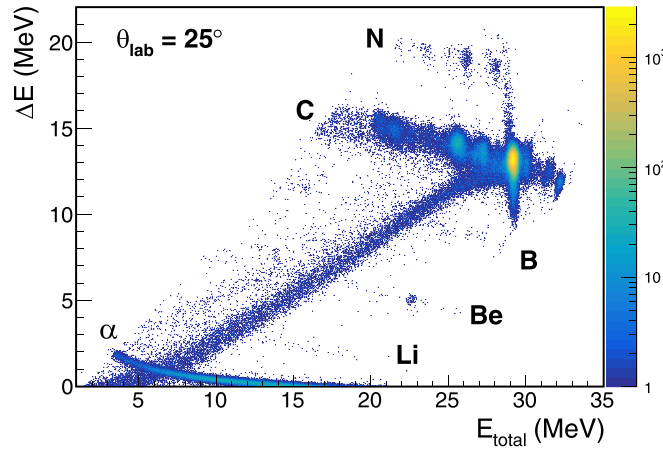

FIG. 1. Calibrated spectrum for the scattering of ^{13}C in ^{27}Al for a bombarding energy of 32 MeV.

corresponds to the elastic scattering in the $^{13}C + ^{27}Al$ system. Inelastic channels corresponds to peaks found at $Q < 0$ whereas the ground-to-ground one-neutron transfer peak lies at $Q = +2.78$ MeV (labelled as $^{28}Al_{g.s.}$ in Fig. 2). Three other peaks have been associated to contaminants (with impurities of less than 2%) introduced to the target foils during manufacturing. According to the kinematics, peaks 1 and 2 (see Fig. 2) are reactions on ^{39}K and ^{32}S target contaminants. Unfortunately, these contaminants are located at the same energy of the ^{28}Al excited states, not being possible to obtain the experimental angular distribution of them. The peak 3 is assigned to a lighter contaminant not clearly determined from kinematics.

A multi-gaussian curve fitted to the experimental spectra has been implemented considering the elastic peak and the known excitation energies of the low-lying states in ^{27}Al (namely, the $1/2^+$ at 0.84 MeV, the $3/2^+$ at 1.01 MeV, and

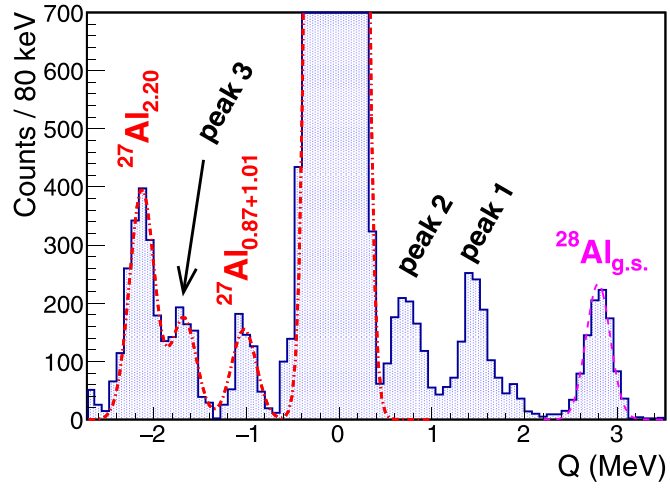

FIG. 2. Q-value spectrum at $\theta_{lab} = 35°$. The elastic, inelastic, and transfer peaks are indicated in the figure. Some contaminants are present in the target: ^{39}K (peak 1), ^{32}S (peak 2), and an unidentified element (peak 3). Data obtained with the ^{27}Al target foil. See text for further details.

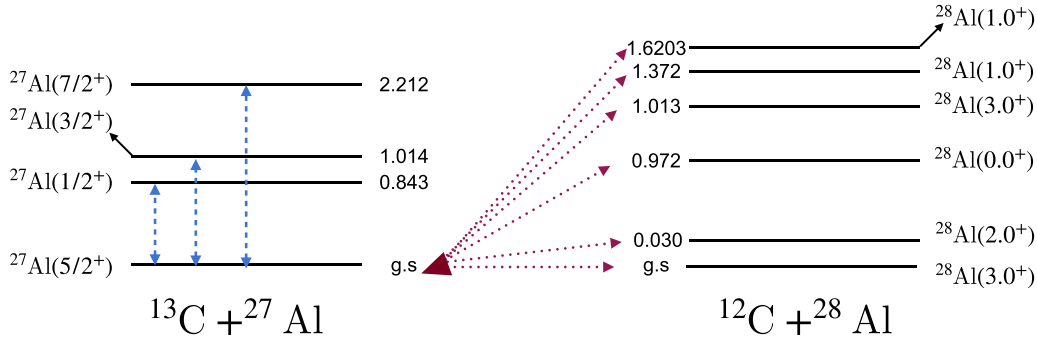

FIG. 3. Schematic view of the excited levels of ^{27,28}Al nuclei considered in the calculations of the present work. For the carbon isotopes, only the g.s. were considered. The dashed blue lines show the adopted couplings between each inelastic state and the g.s. The nuclear transitions $M(E2)(e\ \text{fm}^2)$ intensities adopted may be visualized in Table I. The dotted red lines show the couplings considered in the one-neutron transfer reaction between ^{27,28}Al nuclei. The respective spectroscopic amplitudes and the quantum numbers adopted for each transition may be visualized in Table II.

the $7/2^+$ at 2.21 MeV), fixing the width of the peaks. The energy resolution, defined as the full width half-maximum of the peaks, was 0.38 MeV in our analysis. An additional gaussian peak was included to describe the intruder peak (peak 3). A typical fitted curve obtained from this procedure is represented by the dashed red curve in Fig. 2. This does not allow to distinguish the $1/2^+$ from the $3/2^+$ states in ^{27}Al and therefore we report the integrated cross sections for these two inelastic channels.

Cross sections were determined from the relative yields of the elastic peaks associated with the ^{13}C scattered off by the ^{27}Al and the ^{197}Au foil. A second measurement was carried out at $E_{\text{lab}} = 20$ MeV for normalization and proper evaluation of systematic uncertainties in the measurements. At this low-energy measurement, we have assumed the Rutherford cross sections for the elastic scattering for the $^{13}\text{C} + ^{197}\text{Au}$ system.

III. THEORETICAL FRAMEWORK

The theoretical analysis of the reaction proceeded by incorporating all the relevant states that have been experimentally observed. Furthermore, given that ^{27}Al has a semi-integer spin due to the unpaired nucleon in the proton s shell ($1d_{5/2}$), the impact of the target spin-orbit potential was also investigated. The same study will be applied later to the ^{13}C nucleus with g.s. semi-integer spin of $1/2^-$.

The coupled channel (CC) and coupled reaction channels (CRC) calculations were performed using the code FRESCO [16]. The adopted coupling scheme is illustrated in Fig. 3 guided by the states that are experimentally observed in the Q-value spectrum (see Fig. 2). The calculations involved the following channels: $5/2^+$ (g.s.), $1/2^+$ ($E^* = 0.84$ MeV), $3/2^+$ ($E^* = 1.01$ MeV), and $7/2^+$ ($E^* = 2.21$ MeV) ^{27}Al states. In the CC calculations, only the couplings indicated by the blue arrows were considered whereas in the CRC all couplings (blue and violet arrows) were included. No couplings between channels within the exiting mass partition were considered.

TABLE I. Nuclear transitions included in the coupling scheme, with their respective $M(E2)(e\,\text{fm}^2)$ and deformation lengths δ (fm) adopted.

Initial state	Final state	$M(E2)(e\ \text{fm}^2)$	δ (fm)
$1/2^+$ (0.843 MeV)	$5/2^+$ (g.s)	8.70	0.70
$3/2^+$ (1.014 MeV)	$5/2^+$ (g.s)	12.30	0.99
$7/2^+$ (2.212 MeV)	$5/2^+$ (g.s)	24.08	1.94

In the case of inelastic channels, there are relevant considerations which should be done before proceeding. The $B(E2)$ reduced transition probabilities were obtained from experimental values reported in Ref. [17]. Deformation lengths (δ) were corrected using the adjustment proposed in Ref. [18], which corrects the unrealistic sharp nuclear mass density distribution adopted in the models. This correction is approximately of the order of 20%. The final parameters used in the calculations are summarized in Table I.

The optical potential $V_n(r)$ in the entrance mass partition is given by a real and an imaginary component. The real component consists of $V_{\text{SPP}}(r)$, the double folding São Paulo potential (SPP) [19–21]. For the imaginary optical potential, two methodologies were employed.

In the first, an imaginary short range Woods-Saxon (WS) potential was used to simulate the fusion process. This internal WS potential is included to effectively take into account the absorption of incident flux to fusion and its equation is expressed as

$$V_{WS}(r) = -\frac{V_i}{1 + \exp\left(\frac{r-R}{a_i}\right)} \tag{1}$$

with depth, reduced radius, and diffuseness fixed to $V_i = 50$ MeV, $r_i = 1.0$ fm, and $a_i = 0.2$ fm, respectively. This type of short range WS potential provides reasonable good description for fusion [22].

The second approach consists of using an optical imaginary potential proportional to the double folding SPP was utilized with a normalization factor N_i ranging from 0.1 to 0.3. The imaginary SPP, with an adjustable normalization factor N_i, simulates the effects of possible surface effects not explicitly considered in our coupling scheme.

TABLE II. Table indicating the ^{27,28}Al transitions considered in the CRC calculations. The angular orbital of the valence neutron and its spectroscopic factor ($\mathcal{S}_1$ for the *psdmod* and $\mathcal{S}_2$ for the *psdmwkpn*) obtained by the NUSHELLX code are also displayed in the table. The last column brings the spectroscopic factors ($\mathcal{S}_3$) of Ref. [28].

Initial state	Final state	shell	$\mathcal{S}_1$	$\mathcal{S}_2$	$\mathcal{S}_3$
^{27}Al ($5/2^+$ - g.s.)	^{28}Al (3^+ - g.s.)	$2s_{1/2}$	0.516	0.439	0.61
^{27}Al ($5/2^+$ - g.s.)	^{28}Al (3^+ - g.s.)	$1d_{3/2}$	0.087	0.003	0.11
^{27}Al ($5/2^+$ - g.s.)	^{28}Al (3^+ - g.s.)	$1d_{5/2}$	0.044	0.085	0.17
^{27}Al ($5/2^+$ - g.s.)	^{28}Al (2^+ - 0.030 MeV)	$1d_{3/2}$	0.268	0.272	0.22
^{27}Al ($5/2^+$ - g.s.)	^{28}Al (2^+ - 0.030 MeV)	$2s_{1/2}$	0.358	0.218	0.40
^{27}Al ($5/2^+$ - g.s.)	^{28}Al (2^+ - 0.030 MeV)	$1d_{5/2}$	0.028	0.041	0.14
^{27}Al ($5/2^+$ - g.s.)	^{28}Al (0^+ - 0.972 MeV)	$1d_{5/2}$	0.128	0.204	0.20
^{27}Al ($5/2^+$ - g.s.)	^{28}Al (3^+ - 1.013 MeV)	$1d_{5/2}$	0.033	0.029	0.81
^{27}Al ($5/2^+$ - g.s.)	^{28}Al (3^+ - 1.013 MeV)	$2s_{1/2}$	0.086	0.006	0.06
^{27}Al ($5/2^+$ - g.s.)	^{28}Al (3^+ - 1.013 MeV)	$1d_{3/2}$	0.577	0.521	1.06
^{27}Al ($5/2^+$ - g.s.)	^{28}Al (1^+ - 1.372 MeV)	$1d_{3/2}$	0.309	0.212	0.28
^{27}Al ($5/2^+$ - g.s.)	^{28}Al (1^+ - 1.372 MeV)	$1d_{5/2}$	0.008	0.001	0.20
^{27}Al ($5/2^+$ - g.s.)	^{28}Al (1^+ - 1.6203 MeV)	$1d_{3/2}$	0.002	0.002	–
^{27}Al ($5/2^+$ - g.s.)	^{28}Al (1^+ - 1.6203 MeV)	$1d_{5/2}$	0.032	0.037	–

Figure 4 shows the elastic scattering angular distribution for the $^{13}C + ^{27}Al$ system at $E_{lab} = 32$ MeV. In the figure, the dash-dotted blue curve represents the CC calculation including the above-mentioned excited states in the target nucleus and the short range imaginary WS potential. Clearly, this calculation does not describe the experimental data.

In a further step, a real spin-orbit potential V_{SO} was added to describe the coupling of target spin with its orbital motion. The spin-orbit potential is given by

$$V_{SO}(r) = -\frac{a_{SO}^2}{r}\frac{dV_{WS}(r)}{dr}\langle \vec{l}\cdot\vec{s}\rangle, \quad (2)$$

where a_{SO} is a scaling factor in terms of the pion mass and $V_{WS}(r)$ is the WS potential with depth V_{SO}, reduced radius r_{SO}, and diffuseness a_{SO}. The derivative of $V_{WS}(r)$ results in a surface potential. In the calculations, the r_{SO} and a_{SO} parameters were fixed to 1.20 fm and 0.60 fm, respectively. The depth was varied to reproduce simultaneously the elastic and inelastic experimental angular distributions.

In the elastic channel, this calculation including the spin-orbit potential is represented by the solid black curve in Fig. 4. Results for the inelastic channels are shown in Fig. 5. The best agreement was obtained for $V_{SO} = 1.25$ MeV. It can be noticed that the inclusion of the spin-orbit potential

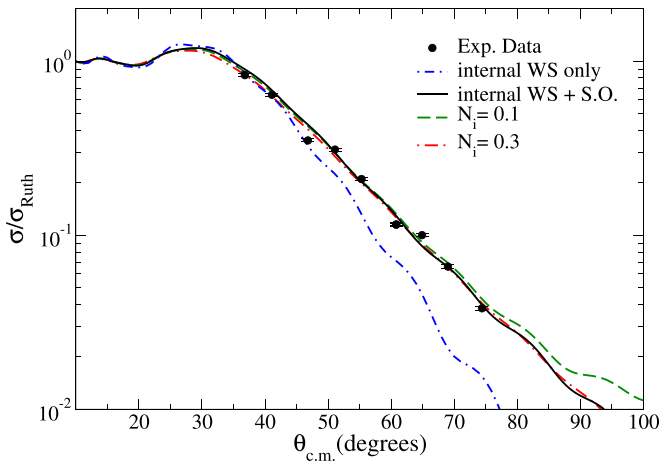

FIG. 4. Elastic scattering angular distribution for $^{13}C + ^{27}Al$ at $E_{lab} = 32$ MeV. The dashed-dotted blue line represents the CC calculation with an internal WS optical potential and no spin-orbit potential. The solid black line is the result of a similar calculation but including the target spin-orbit potential. The dashed green line brings the same coupling scheme and potentials previously mentioned but changing the WS shape of the imaginary potential to a SPP shape with normalization of $N_I = 0.1$. The red dashed-dotted line is similar to the green, but with an imaginary normalization of $N_I = 0.3$.

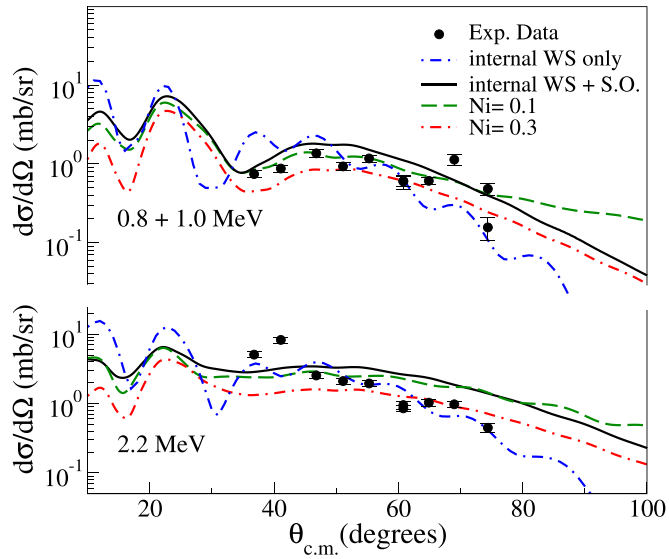

FIG. 5. (Top) Angular distribution of the inelastic scattering cross section for the first excited states of the ^{27}Al ($0.84 + 1.01$). (Bottom) Angular distribution of the inelastic scattering cross section third excited state ^{27}Al (2.21). The calculations performed are the same as Fig. 4.

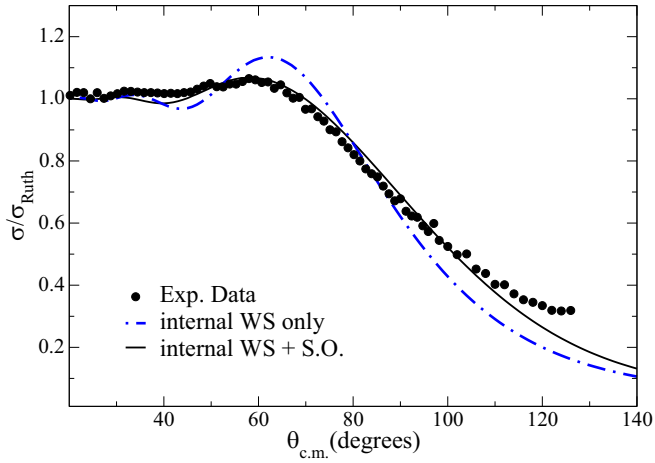

FIG. 6. Angular distribution of the elastic scattering cross section for the $^{12}C + ^{27}Al$ reaction at $E_{lab} = 21$ MeV. The dashed dotted blue line represents a CC calculation with an internal WS optical potential and no spin-orbit effect. The solid black line is the same of the red one but including the target spin-orbit.

provides a reasonable description of the summed inelastic scattering of the $1/2^+$ and $3/2^+$ states. The individual $7/2^+$ inelastic state was also reasonable described by this calculation. Coupled channel calculations considering the same level scheme, the nuclear and the target spin-orbit potential have also been performed including the projectile spin-orbit potential, but no significant effect were observed in the theoretical cross sections. Hence, these results are not shown in Figs. 4 and 5.

The target spin-orbit potential seems to be an important ingredient in modeling the direct reactions for the $^{13}C + ^{27}Al$ system. Similar calculations for the $^{12}C + ^{27}Al$ system at $E_{lab} = 21$ MeV were performed to investigate the effect of the target spin-orbit potential. Experimental data were obtained from Ref. [23] and a comparison with our CC calculations is shown in Fig. 6. The experimental uncertainties have been suppressed in the figure for better visualization of the theoretical calculations of the present work.

The first calculation (dotted-dashed blue line) considers only couplings to the inelastic channels of the target and the imaginary part of the nuclear potential is the internal WS potential. One may visualize from the figure that the data could not be well reproduced by the calculation. Further calculations considering similar values for the spin-orbit effect ($V = 2.3$ MeV, $a = 0.60$ fm, and $r_0 = 1.20$) adopted for the $^{13}C + ^{27}Al$ system are displayed in the figure as a solid black line and show a much better accordance with the data. Both the order of magnitude of the data at the backward region and the flattening of the interference Fresnel peak are well described. The different depth of the spin-orbit potential adopted for the $^{12}C + ^{27}Al$ reaction when compared to the $^{13}C + ^{27}Al$ may result from the different reaction energies in both cases.

In the context of the $^{13}C + ^{27}Al$ reaction, when the same set of potential parameters was applied to both nuclei, the effect of the target one was much more pronounced than that of the projectile. Nonetheless, it is reasonable to argue that different combinations of target and projectile parameters might also be capable of describing the data. In fact, in the case of the $^{13}C + ^{28}Si$ reaction, a calculation considering only the primary inelastic channels and an internal imaginary potential could not describe the data in Ref. [11]. This suggests the potential presence of the spin-orbit effect in the projectile in that case. Therefore, the present findings can be understood as an averaged effect arising from the spin-orbit interaction of the participating nuclei. Since a comprehensive study of the spin-orbit effect is beyond the scope of this work, a simplified calculation involving only the effect in the target was adopted in the further calculations.

The investigation proceeded by examining the impact of different optical potentials within the theoretical framework. Calculations with the same couplings and still using the target spin-orbit potential were performed, but now considering different optical imaginary potentials. Further calculations are shown, using the São Paulo potential as the imaginary term with different normalization factors N_i ranging from 0.1 to 0.3.

In Fig. 4, it is evident that the choice of the N_i normalization had a small effect on the description of the experimental data in the context of the elastic scattering. This suggests that elastic scattering appears to be insensitive to small variations in the adopted imaginary part of the optical potential. A more strong analysis of this sensitivity becomes apparent when considering other channels, such as the inelastic channels, as shown in Fig. 5.

Figure 5 presents a comparison of data and theoretical calculations for the inelastic channels, considering two cases: the summed differential cross sections for $1/2^+$ ($E^* = 0.843$ MeV) and $3/2^+$ ($E^* = 1.014$ MeV) states of ^{27}Al and the individual cross section for the $7/2^+$ ($E^* = 2.212$ MeV) state. The variability in experimental data makes it challenging to definitively assert that any single calculation provides a superior fit over others. In the up, the calculation using the WS imaginary potential results with the best adjustment to the inelastic scattering data. However, for the distribution below, the best fit appears to be for the SPP with $N_i = 0.1$. This suggests that there may be additional surface effects not accounted for in the calculations (which is consistent with all the reaction channels observed in the experimental spectrum of Fig. 1).

This observation is not entirely unexpected, especially considering that ^{27}Al is a deformed nucleus. When comparing the data with that of Ref. [11], it is worth noting that ^{27}Al exhibits a similar behavior to ^{28}Si. Although a WS calculation was not performed for ^{28}Si, the behavior with $N_i = 0.1$ and $N_i = 0.3$ is consistent, corroborating that these nuclei share similar characteristics.

Further calculations also revealed that it is not possible to obtain a good description of the experimental angular distributions using a CC calculation (considering the same coupling scheme) with an imaginary optical potential where the SPP is adopted with a variable N_i normalization, but with no target spin orbit potential included. In this sense, the inclusion of this potential is another indication of the necessity of considering of such effect. Also one should notice that the presence of such effect may only be noticed due to the energy region where the $^{13}C + ^{27}Al$ reaction has been presently done. The $^{16}O + ^{27}Al$ reaction has been previously measured at much

higher bombarding energies ($E_{\rm lab} = 100$ MeV in Ref. [24] and $E_{\rm lab} = 240$ MeV in Ref. [25]), that are much above the Coulomb barrier of the system, meaning that other reaction mechanisms may play an important role and the spin orbit effect will not be so apparent.

After completing the elastic and inelastic analyses of the $^{13}C + ^{27}Al$ reaction, the study proceeded by investigating the one-neutron transfer channel. Before performing the dynamical calculations of this reaction, it was necessary to obtain the appropriate wave functions that describe the valence particle (the neutron in this case) when initially bound to ^{13}C and later to ^{28}Al. To achieve this, a structural calculation was conducted to derive the wave functions of each state and their associated spectroscopic factors ($\mathcal{S}$). This was accomplished using the code NUSHELLX [26]. The spectroscopic information for the $^{12,13}C$ projectile/ejectile was the same adopted in the description of the one-neutron transfer process in the $^{13}C + ^{28}Si$ reaction from Ref. [11].

For the $^{27,28}Al$ nuclei, it was essential to employ the same model space and interactions in the structure calculations. Consequently, a model was chosen that incorporated a ^{4}He as a core, leaving available the $1p_{1/2}$, $1p_{3/2}$, $1d_{3/2}$, $1d_{5/2}$, and $2s_{1/2}$ orbitals for the remaining particles. Two nuclear interactions were used for the structural calculations: the first, proposed in Ref. [12] (referred to as *psdmod* in the NUSHELLX code), and the latter, a modified version presented in Ref. [13] (labeled as *psdmwkpn*). To check the appropriateness of these interactions in describing the target and recoiling nuclei, an examination of the spin-parity and associated excitation energy of each level was conducted. The calculations performed with both interactions resulted that the order of the excited levels in the $^{27,28}Al$ nuclei was well reproduced, and the excitation energy of these levels was accurately described within a 200 keV range.

Subsequently, a coupled reaction channel calculation was performed, which included the one-neutron transfer (1NT) reaction channel in the previous CC approach. The spectroscopic information obtained earlier was used in this CRC calculation. The coupling scheme for the $^{27,28}Al$ overlap considered only the feeding from the ground state of the target nucleus. The inclusion of overlaps considering the couplings of its excited levels with ^{28}Al would involve an excitation followed by the transfer, a second-order process expected to have a minimal contribution in this scenario. The CRC calculation was implemented using the code FRESCO. The spectroscopic factors ($\mathcal{S}$) for the two interactions adopted in the NUSHELLX code, along with relevant spectroscopic information (n, ℓ, and j quantum numbers), can be found in Table II.

To perform the CRC calculations, a matching radius of 40 fm was employed, and up to 250 partial waves were considered. For the entrance partition, the potential utilized was the SPP with a normalization factor of $N_i = 0.1$ for its imaginary part. However, for the exit partition, where no elastic data was available for the $^{12}C + ^{28}Al$ reaction, the standard São Paulo systematics [27] was followed, involving the use of the SPP with a normalization of $N_i = 0.78$ for the imaginary part. Given the greater confidence in the optical potential adopted for the entrance partition, as it could be compared to

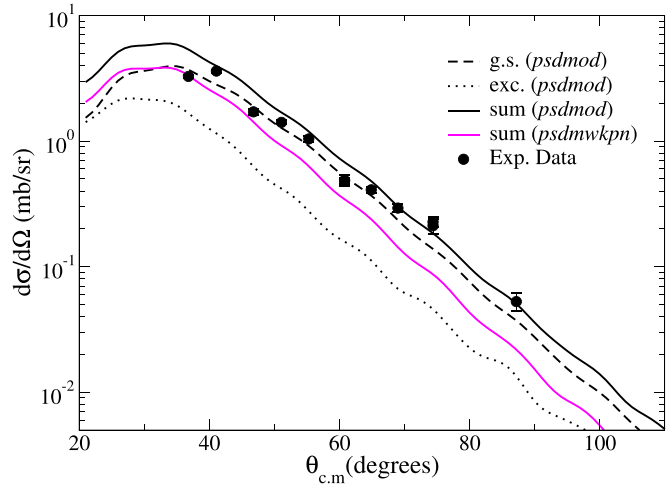

FIG. 7. One neutron transfer angular distribution for $^{13}C + ^{27}Al \rightarrow ^{12}C + ^{28}Al$ at the bombarding energy of 32 MeV. The solid magenta line is a CRC calculation using the $\mathcal{S}$ values obtained with *psdmwkpn* interaction. The solid black line brings the $\mathcal{S}$ values obtained with the *psdmod* interaction. The dashed black line shows the individual contribution of the transfer to the g.s. of ^{28}Al, while the dotted black line shows the contribution for its first excited state. The individual contributions displayed is made solely for the *psdmod* interaction.

experimental data, a prior representation with a complex remnant was adopted.

The neutron-core potentials used consisted of a real WS shape with a diffuseness parameter (a) of 0.60 fm and a reduced radius (r_0) of 1.30 fm. The depth of these potentials was adjusted to match the expected binding energy of each state. Additionally, a spin-orbit component (with the same parameters previously adopted) was introduced to account for the neutron-^{27}Al interaction. Since the experimental spectra of the reaction indicated that only the low-lying states of ^{28}Al were populated, the coupling scheme considered only the excited states up to approximately 1.6 MeV in the recoiling nucleus.

The analysis of the 1NT spectra reveals a peak consistent with the transition to the 3^+ (ground state) and the 2^+ ($E^\star = 0.03$ MeV) excited state of ^{28}Al. Due to the inability to experimentally differentiate between these two states, the reported differential cross sections are the sum of both states. Figure 7 illustrates the comparison between the data and CRC calculations performed using the previously explained framework, but considering the spectroscopic factors calculated with the *psdmwkpn* and *psdmod* interactions. It is evident that the *psdmod* interaction provides a better description of the experimental data than the *psdmwkpn* one. This can be attributed to the fact that, as observed in Table II, the *psdmod* spectroscopic factors are generally larger than those obtained with *psdmwkpn*, leading to higher cross sections that best fit the data. A similar trend was observed in the $^{13}C + ^{28}Si$ reaction, further reinforcing the similarity between these nuclei. Additionally, there is a strong indication that the *psdmod* interaction should be the preferred choice for describing nuclear properties in this mass region. One may also visualize from

the figure that the contribution of the one-neutron transfer to the g.s. seems to be the dominant contribution for the summed cross section, representing, on average, around 70% of the total theoretical value.

The spectroscopic factors ($\mathcal{S}$) obtained via our NUSHELLX calculation were compared with those experimentally determined using a (d, p) reaction from Ref. [28] (see Table II). It is apparent that the latter values are larger than those obtained with code NUSHELLX. Reference [28] obtained these values by experimentally adjusting the spectroscopic amplitudes to reproduce data using a distorted wave Born approximation (DWBA) calculation. However, such a procedure can lead to incorrect amplitude values since it may introduce a component from the nuclear reaction mechanism into the structural factor. In the present method, structural and dynamic mechanisms are calculated separately and then combined, ensuring that both calculations and the effects arising from each are accurately treated to provide a correct description of the data.

IV. CONCLUSIONS

This article presents a successful measurement of the $^{13}C + ^{27}Al$ reaction at a bombarding energy of $E = 32$ MeV. Experimental data encompassing elastic scattering, low-lying inelastic channels ($1/2^+ + 3/2^+$ at $E^\star \approx 0.9$ MeV and $7/2^+$ at $E^\star = 2.2$ MeV), and one-neutron stripping transfer to the ground state have been obtained. The coupling scheme includes these excited states, and a nuclear optical internal WS potential was employed in CC calculations to simulate the fusion process. However, the calculated angular distributions for the elastic and inelastic channels did not reproduce the experimental data, suggesting the need to consider additional effects or reaction mechanisms.

To improve the agreement between theory and experiment, the spin-orbit potential for the target was incorporated into the model. A constrained comparison of this revised theoretical framework with the experimental data revealed that the spin-orbit effect in the target plays a crucial role in the reaction. The inclusion of this effect allowed for a considerably better description of both elastic and inelastic data, bringing the angular distributions into the same order of magnitude as the experimental measurements. Interestingly, the inclusion of the spin-orbit effect for the projectile did not result in any observable effects on the angular distributions, suggesting that the effect of the heavier nucleus (target) is more significant than that of the lighter one (projectile).

To account for potential surface effects not explicitly included in the calculations, the imaginary potential was modified to adopt a São Paulo shape for the imaginary part of the optical potential normalization in the range of $N_I = 0.1$–0.3. These adjustments appeared to provide a better description of data, particularly for the measured inelastic states. The elastic scattering angular distribution remained relatively unaffected by this change. The experimental inelastic data exhibited significant angular distribution variations, attributed to the challenge of extracting it from the experimental spectra, given the presence of other reaction mechanisms and contaminants in the target. This theoretical approach closely resembles the one employed for the $^{13}C + ^{28}Si$ reaction in Ref. [11], further indicating the similarity between both nuclei.

Structure calculations using the NUSHELLX code were made with two different nuclear interactions, labeled as *sdmwkpn* and *psdmod* in the code. While both interactions yielded similar descriptions of the $^{27,28}Al$ nuclei in terms of spin, parity, and energy levels, they exhibited different spectroscopic values. In CRC calculations for the one-neutron transfer process, the *psdmod* interaction outperformed the other when it came to describing the experimental data. Once again, this result aligns with the findings from Ref. [11] for the $^{13}C + ^{28}Si$ reaction and provides strong evidence that this approach is well suited for describing nuclei in this mass region.

ACKNOWLEDGMENTS

This project has received funding from CNPq, FAPERJ, FAPESP, and CAPES and from INCT-FNA (Instituto Nacional de Ciência e Tecnologia-Física Nuclear e Aplicações) (Proc. No. 464898/2014-5). V.A.B.Z. thanks CNPq (Proc. No. 304750/2021-2) for the financial support. R.L. thanks CNPq (Proc. No. 317451/2021-9) for the financial support. J.C.Z. thanks FAPESP (Grants No. 2018/04965-4 and No. 16/17612-7) for the financial support. We would also like to thank the technical staff of LAFN for assisting in the maintenance and operation of the accelerator. This research has also used resources of the LAMFI-USP.

[1] M. C. Mermaz, C. A. Whitten, J. W. Champlin, A. J. Howard, and D. A. Bromley, Phys. Rev. C **4**, 1778 (1971).
[2] R. Peterson, C. Fields, R. Raymond, J. Thieke, and J. Ullman, Nucl. Phys. A **408**, 221 (1983).
[3] K. Pearce, N. Clarke, R. Griffiths, P. Simmonds, D. Barker, J. England, M. Mannion, and C. Ogilvie, Nucl. Phys. A **467**, 215 (1987).
[4] C. J. Forrest, A. Deltuva, W. U. Schroder, A. V. Voinov, J. P. Knauer, E. M. Campbell, G. W. Collins, V. Yu. Glebov, O. M. Mannion, Z. L. Mohamed *et al.*, Phys. Rev. C **100**, 034001 (2019).
[5] F. Cappuzzello, C. Agodi, M. Cavallaro, D. Carbone, S. Tudisco, D. Lo Presti, J. R. B. Oliveira, P. Finocchiaro, M. Colonna, D. Rifuggiato *et al.*, Eur. Phys. J. A **54**, 72 (2018).
[6] A. Kundu, S. Santra, A. Pal, D. Chattopadhyay *et al.*, Phys. Rev. C **95**, 034615 (2017).
[7] V. A. B. Zagatto, J. Lubian, L. R. Gasques, M. A. G. Alvarez, L. C. Chamon, J. R. B. Oliveira, J. A. Alcántara-Núñez, N. H. Medina, V. Scarduelli, A. Freitas, I. Padron, E. S. Rossi, and J. M. B. Shorto, Phys. Rev. C **95**, 064614 (2017).
[8] V. A. B. Zagatto, M. Gómez-Ramos, L. R. Gasques, A. M. Moro, L. C. Chamon, M. A. G. Alvarez, V. Scarduelli, J. P.

Fernández-Garcia, J. R. B. de Oliveira, A. Lépine-Szily, and A. Arazi, Phys. Rev. C **106**, 014622 (2022).
[9] J. K. L. Chaves, L. R. Gasques, L. C. Chamon, V. Scarduelli, A. Lépine-Szily, W. A. Y. Hatano, and V. A. B. Zagatto, Phys. Rev. C **108**, 044602 (2023).
[10] V. A. B. Zagatto, B. R. Gonçalves, and D. R. Mendes Junior, Phys. Rev. C **107**, 044604 (2023).
[11] R. Linares, C. C. Seabra, V. A. B. Zagatto, V. Scarduelli, L. Gasques, L. C. Chamon, B. R. Gonçalves, D. R. Mendes Junior, and A. Lépine-Szily, Phys. Rev. C **101**, 014611 (2020).
[12] Y. Utsuno and S. Chiba, Phys. Rev. C **83**, 021301(R) (2011).
[13] R. Meharchand, R. G. T. Zegers, B. A. Brown, S. M. Austin, T. Baugher, D. Bazin, J. Deaven, A. Gade, G. F. Grinyer, C. J. Guess *et al.*, Phys. Rev. Lett. **108**, 122501 (2012).
[14] R. Linares, C. C. Seabra, V. A. B. Zagatto, F. Cappuzzello, M. Cavallaro, D. Carbone, C. Agodi, L. M. Fonseca, and J. R. B. Oliveira, Phys. Rev. C **108**, 014619 (2023).
[15] L. R. Gasques, A. S. Freitas, L. C. Chamon, J. R. B. Oliveira, N. H. Medina, V. Scarduelli, E. S. Rossi, Jr., M. A. G. Alvarez, V. A. B. Zagatto, J. Lubian, G. P. A. Nobre, I. Padron, and B. V. Carlson, Phys. Rev. C **97**, 034629 (2018).
[16] I. J. Thompson, Comput. Phys. Rep. **7**, 167 (1988).
[17] K. Q. Robert, J. R. Linn, and F. E. Durham, Nucl. Instrum. Methods **79**, 251 (1970).
[18] L. C. Chamon and B. V. Carlson, Nucl. Phys. A **846**, 1 (2010).
[19] M. A. Cândido Ribeiro, L. C. Chamon, D. Pereira, M. S. Hussein, and D. Galetti, Phys. Rev. Lett. **78**, 3270 (1997).
[20] L. C. Chamon, D. Pereira, M. S. Hussein, M. A. Candido Ribeiro, and D. Galetti, Phys. Rev. Lett. **79**, 5218 (1997).
[21] L. C. Chamon, B. V. Carlson, L. R. Gasques, D. Pereira *et al.*, Phys. Rev. C **66**, 014610 (2002).
[22] L. F. Canto, P. R. S. Gomes, R. Donangelo, and M. S. Hussein, Phys. Rep. **424**, 1 (2006).
[23] S. Hamada, N. Burtebayev, K. A. Gridnev, and N. Amangeldi, Phys. Scr. **84**, 045201 (2011).
[24] V. A. B. Zagatto, F. Cappuzzello, J. Lubian, M. Cavallaro, R. Linares, D. Carbone, C. Agodi, A. Foti, S. Tudisco, J. S. Wang, J. R. B. Oliveira, and M. S. Hussein, Phys. Rev. C **97**, 054608 (2018).
[25] L. M. Fonseca, R. Linares, V. A. B. Zagatto, F. Cappuzzello, D. Carbone, M. Cavallaro, C. Agodi, J. Lubian, and J. R. B. Oliveira, Phys. Rev. C **100**, 014604 (2019).
[26] B. A. Brown and W. D. M. Rae, Nucl. Data Sheets **120**, 115 (2014).
[27] M.A.G. Alvarez Jr., L. C. Chamon, M. S. Hussein, D. Pereira, L. R. Gasques, E. S. Rossi, Jr., and C. P. Silva, Nucl. Phys. A **723**, 93 (2003).
[28] T. P. G. Carola and J. G. Van Der Baan, Nucl. Phys. A **173**, 414 (1971).